Phys Chem Minerals (2014) 41:527–535
DOI 10.1007/s00269-014-0664-2

ORIGINAL PAPER

The strength of ruby from X-ray diffraction under non-hydrostatic compression to 68 GPa

Haini Dong · Susannah M. Dorfman · Jianghua Wang · Duanwei He · Thomas S. Duffy

Received: 16 October 2013 / Accepted: 26 February 2014 / Published online: 15 March 2014

Abstract Polycrystalline ruby (α-Al_2O_3:Cr^{3+}), a widely used pressure calibrant in high-pressure experiments, was compressed to 68.1 GPa at room temperature under non-hydrostatic conditions in a diamond anvil cell. Angle-dispersive X-ray diffraction experiments in a radial geometry were conducted at beamline X17C of the National Synchrotron Light Source. The stress state of ruby at high pressure and room temperature was analyzed based on the measured lattice strain. The differential stress of ruby increases with pressure from ~3.4 % of the shear modulus at 18.5 GPa to ~6.5 % at 68.1 GPa. The polycrystalline ruby sample can support a maximum differential stress of ~16 GPa at 68.1 GPa under non-hydrostatic compression. The results of this study provide a better understanding of the mechanical properties of this important material for high-pressure science. From a synthesis of existing data for strong ceramic materials, we find that the high-pressure yield strength correlates well with the ambient pressure Vickers hardness.

Keywords Ruby · High-pressure · Radial X-ray diffraction · Strength

H. Dong (✉) · J. Wang · D. He
Institute of Atomic and Molecular Physics, Sichuan University, Chengdu 610065, China
e-mail: hdong1229@gmail.com

D. He
e-mail: duanweihe@scu.edu.cn

H. Dong · S. M. Dorfman · T. S. Duffy
Department of Geosciences, Princeton University, Princeton, NJ 08544, USA
e-mail: duffy@princeton.edu

H. Dong
Institute of Geophysics, Chinese Academy of Sciences, Guiyang 550002, China

S. M. Dorfman
Earth and Planetary Science Laboratory, Ecole polytechnique fédérale de Lausanne, Station 3, 1015 Lausanne, Switzerland

Introduction

The strength and mechanical properties of hard ceramic materials are required for understanding their stability and for their applications under extreme static and dynamic mechanical stresses and high pressures (Duffy 2007). Aluminum oxide, Al_2O_3, has many useful mechanical properties such as high hardness, wear resistance, and fracture toughness, combined with chemical inertness and thermal stability. Ruby (α-Al_2O_3:Cr^{3+}) is aluminum oxide (corundum, sapphire) doped with a small quantity (~0.1 %) of trivalent chromium (Chervin et al. 2001). It has been a widely used pressure standard for static high-pressure experiments in diamond anvil cells (DAC) ever since the development of the ruby fluorescence pressure scale in the 1970s (Forman et al. 1972; Piermarini et al. 1975; Mao et al. 1978). The use of ruby fluorescence for in situ stress measurements in high-pressure experiments played a major role in accelerating the widespread application of the DAC. Given the importance of ruby in high-pressure science, complete characterization of this fundamental material is needed.

Static high-pressure studies of the elastic and plastic compression behavior of corundum and ruby remain limited (Jephcoat et al. 1988; Meade and Jeanloz 1990; Funamori et al. 1994). Many recent high-pressure studies on ruby have focused on improved calibration of the pressure-induced shift of fluorescence lines (Mao et al. 1978; Jephcoat et al. 1988; Eggert et al. 1989; Holzapfel 2003; Dewaele et al.

2004; Chijioke et al. 2005; Dorogokupets and Oganov 2007), extending the scale up to the Mbar range (Eggert et al. 1989; Chijioke et al. 2005). Other studies have examined the sensitivity of the ruby fluorescence signal to non-hydrostatic stress (Piermarini et al. 1975; Chai and Brown 1996; Klotz et al. 2009; Nellis et al. 2010). Meade and Jeanloz (1990) measured pressure gradients across ruby under non-hydrostatic stress to determine that the yield strength of ruby reaches ~12 GPa at 70 GPa. Under dynamic compression, Al_2O_3 was reported to exhibit a yield strength of 21 GPa at 100 GPa (Reinhart and Chhabildas 2003; Reinhart et al. 2006). The deformation behavior of materials under extreme conditions can be measured more directly in situ by radial X-ray diffraction (RXRD) (Singh et al. 1998a, b; Duffy et al. 1999a, b; Kavner and Duffy 2001; Merkel et al. 2002; Shieh et al. 2004) together with lattice strain theory (Singh et al. 1998a; Singh 2004, 2009). RXRD enables us to observe lattice strain of compressed samples in a wide range of orientations relative to a non-hydrostatic stress field. In this study, we use angle-dispersive RXRD (Singh 1993; Merkel et al. 2002) to observe the non-hydrostatic compression behavior of polycrystalline ruby up to 68.1 GPa in a diamond anvil cell and provide new constraints on the mechanical properties of ruby under extreme non-hydrostatic conditions.

Theoretical background

Lattice strain theory (Singh 1993, 2004, 2009; Singh et al. 1998a) describes the variation of lattice strain in a crystal as a function of orientation relative to the applied stress. The stress state in a polycrystalline sample in a diamond anvil cell is approximately uniaxial, with a maximum stress along the DAC loading axis, σ_3, and a minimum stress in the radial direction, σ_1. The difference between σ_3 and σ_1 is the macroscopic differential stress, t. The observed d spacing (d_m) from RXRD measurements can be expressed as a function of the angle ψ between the DAC loading axis and diffraction plane normal (hkl):

$$d_m(hkl) = d_p(hkl)\left[1 + \left(1 - 3\cos^2\right)Q(hkl)\right], \quad (1)$$

where $d_p(hkl)$ is the d spacing resulting from the hydrostatic component of stress $\sigma_p = (2\sigma_1 + \sigma_3)/3$, and $Q(hkl)$ is the orientation-dependent lattice strain (Singh 2004, 2009):

$$Q(hkl) = t \Big/ \left[6G^X(hkl)\right]. \quad (2)$$

G^X is the diffraction shear modulus for the (hkl) lattice planes which is given by:

$$\left[G^X(hkl)\right]^{-1} = \left\{\left[G_R^X(hkl)\right]^{-1} + (1-\alpha)[G(V)]^{-1}\right\}. \quad (3)$$

$G_R^X(hkl)$ is the diffraction shear modulus assuming stress continuity (Reuss limit) across the grain boundaries and $G(V)$ denotes the aggregate shear modulus under strain continuity (Voigt bound) across the interfaces between the crystallites, respectively. α is the parameter specifying the degree of stress and strain continuity across grains in the polycrystalline sample. Equation (1) indicates a linear relation between d_m and $1 - 3\cos^2\psi$. The slope of the fit yields the product $d_p(hkl)Q(hkl)$. The differential stress in the sample can be given by (Singh et al. 1998a, b):

$$t = 6G < Q(hkl) > f(x), \quad (4)$$

where $<Q(hkl)>$ represents the average value of $Q(hkl)$ over all observed peaks and G is the aggregate shear modulus of a randomly oriented polycrystalline sample. In the diffraction geometry used here, t is nearly insensitive to the value of α. $f(x)$ is a function of α and elastic anisotropy which has been verified to be close to 1 for solids over a wide range of α and x values (Singh et al. 1998a, 2012; Singh 2009; Singh and Liermann 2011). The supported differential stress given by Eq. (4) is a lower bound to the yield strength, Y, of the sample under pressure.

Experiment

Polycrystalline ruby powder (average grain size ~3–30 μm, annealed) was ground to ~0.5-μm grain size and loaded into a 100-μm-diameter hole of a Be gasket in a diamond anvil cell. The gasket hole shrank by ~40 % under compression. The gasket was pre-indented to ~30-μm thickness. A ~15-μm-diameter Pt foil placed on top of the sample within 5 μm of the sample center served as a pressure marker as well as a positional reference. A symmetric diamond anvil cell with a culet size of 300 μm was used to compress the sample. No pressure medium was used resulting in non-hydrostatic conditions in the sample chamber. Approximately 30 min was allowed for stress equilibration after each compression step. Two separate experiments were conducted. One sample was compressed up to 68.1 GPa in ~5–10 GPa steps, and an additional sample was compressed to 37.2 GPa in ~5 GPa steps.

Angle-dispersive X-ray diffraction in a radial geometry (Singh et al. 1998a; Duffy et al. 1999b; Merkel et al. 2002) was performed at the X17C beamline of the National Synchrotron Light Source at Brookhaven National Laboratory. The diamond anvil cell was oriented with the diamond axis perpendicular to the incoming X-ray beam. X-rays of wavelength 0.4066 Å were focused to 25 μm × 30 μm using Kirkpatrick–Baez mirrors. The diffracted intensity was recorded with a Rayonix SX-165 CCD detector. Typical data collection time was ~30 min. The 2-D diffraction images were analyzed with the program FIT2D (Hammersley et al.

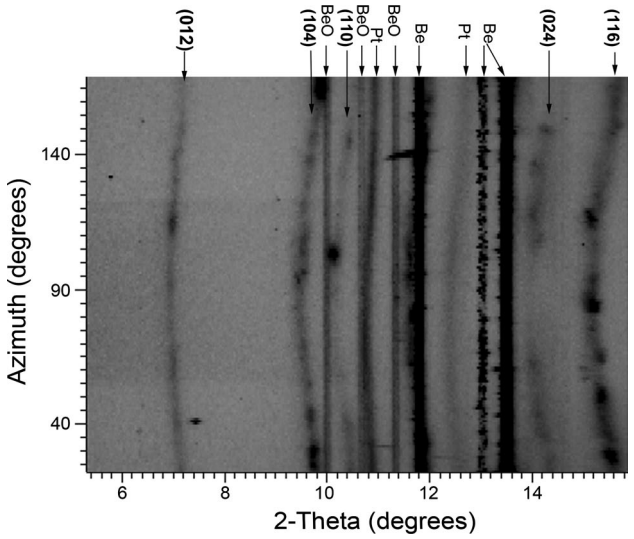

Fig. 1 Unrolled diffraction image at 68.1 GPa from FIT2D. The sinusoidal variations in diffraction lines reflect variations in lattice strain with azimuthal angle

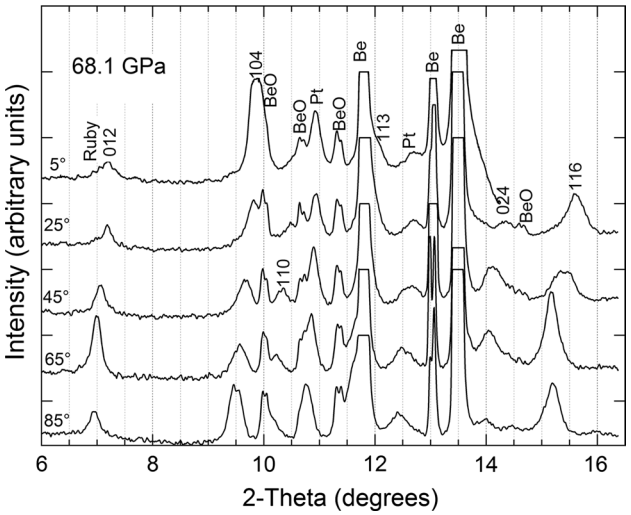

Fig. 2 Diffraction patterns integrated along 5° angular ranges around different azimuthal angles of ruby at 68.1 GPa. Diffraction peaks of ruby (with *hkl*), Pt, Be, and BeO are identified on the figure. The intense Be peaks have been truncated

1996) after the detector distance and orientation was calibrated with a CeO_2 standard. Strong diffraction spots were masked in the software and do not affect the subsequent analysis. Due to spatial restrictions in the X17C station, the CCD detector is mounted in an off-center position, and the complete 360° Debye–Scherrer rings could not be recorded. Instead, the measured azimuthal angle, δ, ranged from ~10° to 180° for diffraction angle, 2θ, up to 22°. At all pressure steps, the (012), (104), (110), (024), and (116) diffraction peaks of ruby were detectable, but the (110) and (024) diffraction peaks were weaker and overlapped by other peaks at some pressures, so they were not used for lattice parameter determination or in the lattice strain analysis. The ψ angle between the diffraction plane normal and loading axis can be calculated from $\cos\psi = \cos\theta \sin\delta$ (Merkel et al. 2002). Pressure was calculated from the equation of state of Pt (Fei et al. 2007) using the unit cell volume from the (111) peak of Pt at $\psi = 54.7°$.

Results and discussion

Non-hydrostatic lattice strain is observed in the sinusoidal variations of ruby and Pt diffraction lines with azimuthal angle (Fig. 1). The minimum compression is observed at azimuthal angle, $\delta = 90°$, perpendicular to the diamond cell loading direction. The diffraction peaks of ruby display larger distortions with azimuthal angle in their Debye rings than Pt, indicating larger lattice strain in ruby than Pt under the same stress. Intensity changes along the diffraction rings, i.e., texture, are due to the crystal preferred orientation (Merkel et al. 2002). While the ruby lines show some spottiness due to a few larger grain sizes, no systematic preferred orientation of ruby grains was observed and a random texture was assumed.

The diffraction patterns were cut into small arcs of 5° azimuthal intervals from $\delta = 0$–90° and integrated with FIT2D to produce a one-dimensional diffraction pattern. Figure 2 presents representative integrated diffraction patterns at 68.1 GPa at selected azimuthal angles. The diffraction peaks shift to larger 2θ at smaller δ corresponding to smaller d spacing in the maximum stress direction. The integrated diffraction patterns were fitted individually with Voigt profiles and a linear background function using the program PeakFit. Figure 3 shows the variation of d spacing of the (012), (104), and (116) lines of ruby with $1 - 3\cos^2\psi$ at selected pressures. Linear variations are observed as expected between the measured d spacing and $1 - 3\cos^2\psi$. The increase in slope with pressure reflects the increase in Q resulting from the increase in differential stress, t, with compression. The lattice strain $Q(hkl)$ can be obtained directly from these linear relations via Eq. (1). The obtained lattice strains for (012), (104), and (116) reflections and their average at different pressures are shown in Fig. 4. At lower pressures, the lattice strain for (116) tends to be systematically higher than the others while the Q value for the (012) peak is the lowest. This reflects some degree of stress anisotropy in ruby, but the differences in lattice strain among the three lines are not very large and they decrease with compression.

If the differential stress reaches its limiting value, i.e., the high-pressure yield strength, then $6 < Q(hkl) >= t/G$ will reflect the ratio of yield strength to shear modulus (He et al. 2004) [assuming $f(x) = 1$]. This ratio,

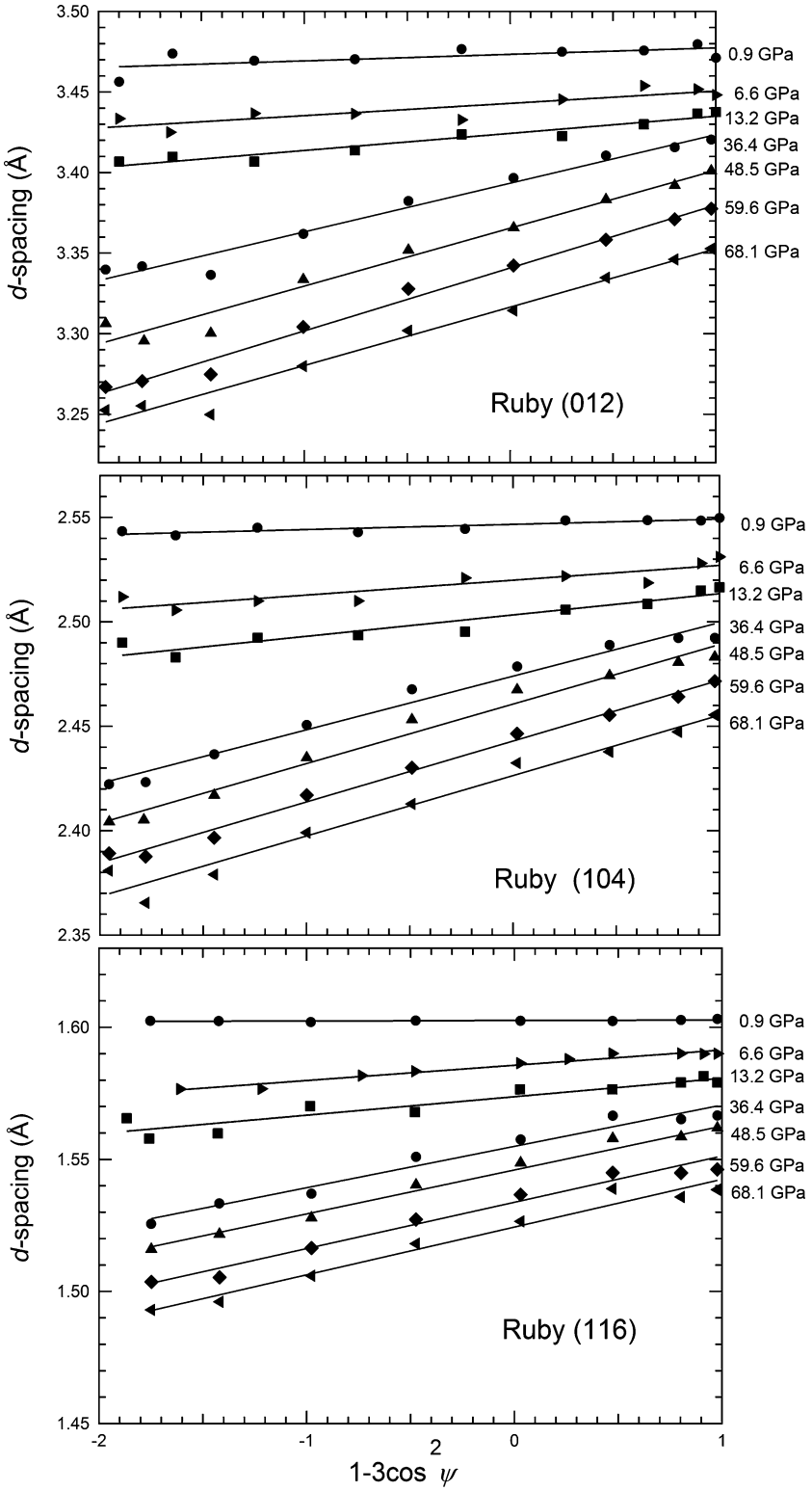

Fig. 3 Dependence of observed *d* spacing versus 1-3cos$^2\psi$ for the (012), (104), and (116) diffraction lines of ruby at selected pressures. The *solid lines* are least-squares fits to the data

$t/G = 6 < Q(hkl) >$, increases strongly with pressure to ~20 GPa and then increases more gradually at higher pressures (Fig. 5a). An initial linear increase in t/G followed by a flattening at higher pressures has been observed previously in radial diffraction studies of other materials such as c-Si_3N_4 (Kiefer et al. 2005). Our interpretation of this is that ruby starts to yield at ~20 GPa. The increase in t/G with pressure above the yield point indicates that the strength increases more rapidly than the shear modulus under compression, indicating significant work hardening (Kiefer

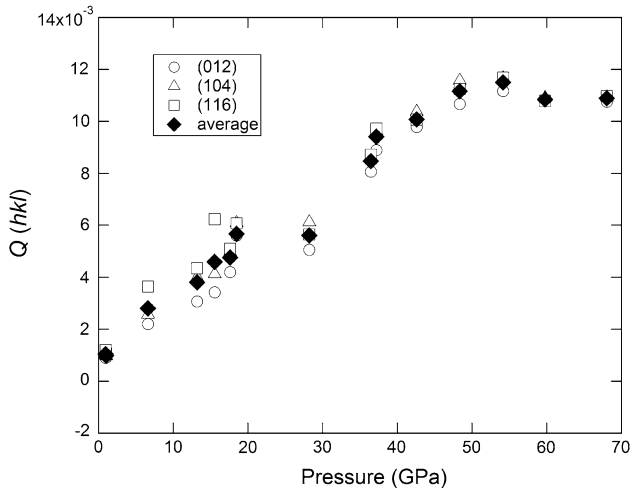

Fig. 4 Lattice strain $Q(hkl)$ for (012), (104), and (116) reflections of ruby and their average value versus pressure

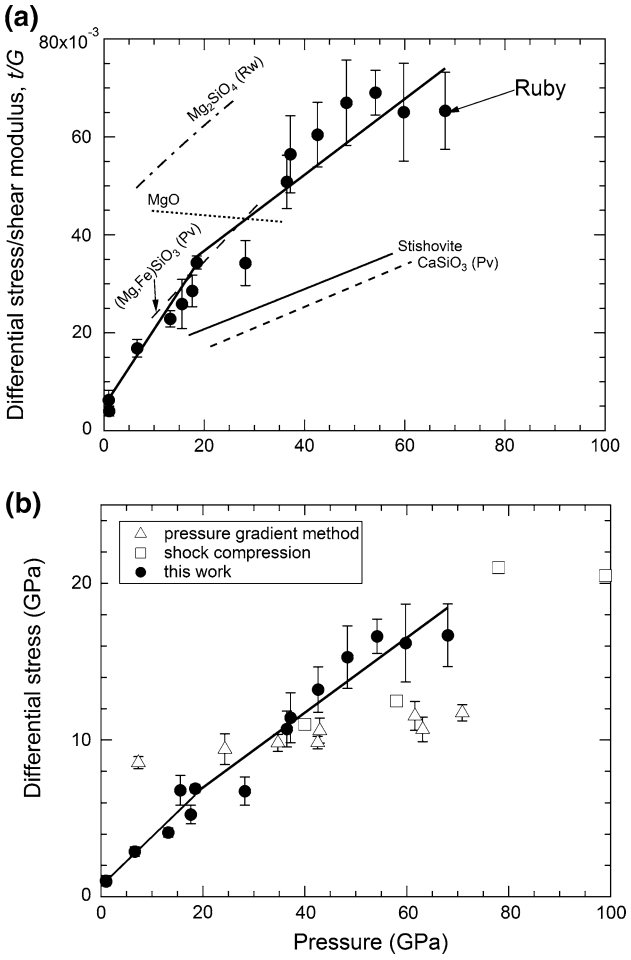

Fig. 5 **a** Ratio of differential stress to shear modulus (t/G) as a function of pressure. *Solid circles* ruby from this study; *solid lines* linear fits to the present data. t/G values for selected geological materials are shown for comparison. *Rw* ringwoodite, *Pv* perovskite. **b** Differential stress of ruby as a function of pressure. *Solid circles* this work; *open triangles* pressure gradient method (Meade and Jeanloz 1990); *open squares* shock wave data (Reinhart and Chhabildas 2003). *Solid lines* linear fits to the present data

et al. 2005). Figure 5a compares t/G for ruby with measurements by radial diffraction of other oxides and silicates of geophysical relevance. The t/G values for ruby, MgO (Merkel et al. 2002), and (Mg, Fe)SiO_3-perovskite (Merkel et al. 2003) lie between the higher value for Mg_2SiO_4-ringwoodite (Kavner and Duffy 2001), and lower values for stishovite (Shieh et al. 2002) and $CaSiO_3$-perovskite (Shieh et al. 2004).

Differential stresses in ruby were determined by extrapolating the shear modulus of ruby to high pressure using its ambient value ($G_0 = 163$ GPa) and its pressure derivative $dG/dP = 1.64$–1.79 as determined by ultrasonic measurements (Chung and Simmons 1968; Gieske and Barsch 1968). The uncertainty in dG/dP leads to ~5 GPa uncertainty in the shear modulus, and this adds ~1 GPa uncertainty to the uncertainty in t [Eq. (4)] at the highest pressures. The differential stress supported by ruby with pressure determined in this study and previous work is shown in Fig. 5b. The maximum differential stress of ruby is ~16 GPa equivalent to ~6.5 % of the shear modulus at 68.1 GPa. The differential stress of ruby in our DAC experiments follows a similar trend with pressure as those from shock wave measurements of aluminum oxide (Reinhart and Chhabildas 2003). This is surprising as shock experiments have strain rates that are orders of magnitude higher than static DAC studies, and strength is known to be rate dependent. The observed agreement may simply be fortuitous as the strength of a material may depend on a number of additional factors including total strain, temperature, and sample microstructure. Further work is needed to better understand the variation of strength in Al_2O_3 for different types of experiments at these high pressures. Previously reported values for ruby in the diamond anvil cell using the pressure gradient method (Meade and Jeanloz 1990) are also shown in Fig. 6. In the pressure gradient technique, the yield strength, Y, (or differential stress in the event that yielding has not occurred) is determined from the measured radial pressure gradient, dP/dr, and the sample thickness, h, as: $t = h(dP/dr)$ (Meade and Jeanloz 1988, 1990). In our study, the pressure dependence of the differential stress is much greater than in the previous DAC measurements, resulting in much higher strength values at higher pressures. The pressure gradient technique requires knowledge of sample thickness which is not directly measured in these experiments. The results may also be affected by anvil deformation or slip at the diamond–sample interface (Vignes et al. 2013). The differential stress of ~5 GPa at around 10 GPa of ruby from this study is consistent with

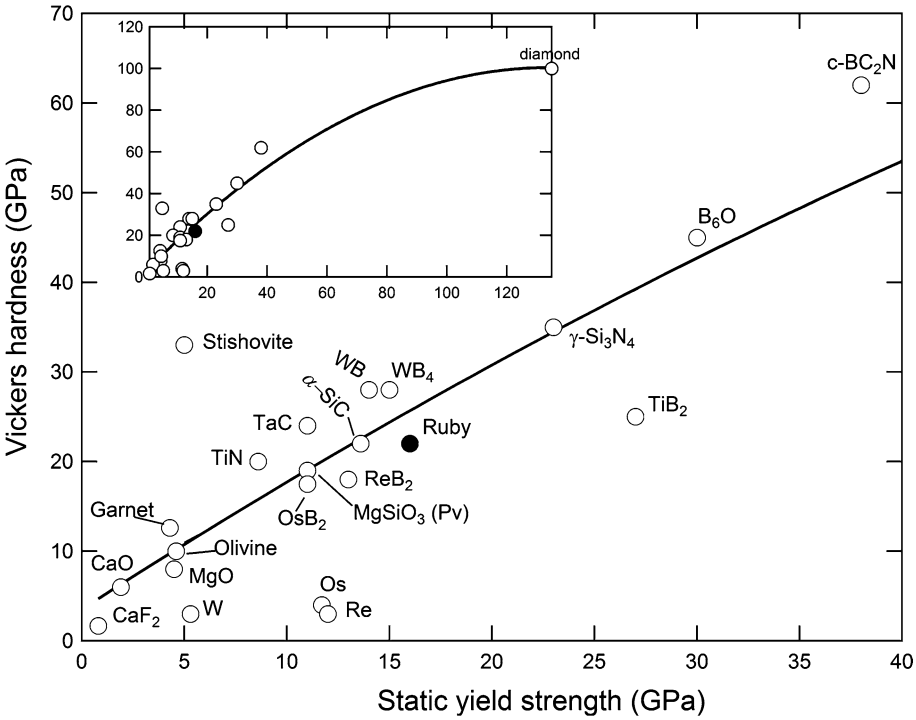

Fig. 6 Vickers hardness versus high-pressure yield strength for selected ceramic materials and metals from static radial X-ray diffraction measurements. The *solid lines* are polynomial fits to the data. Os, W, and Re are not included in the fit. The *inset* shows the yield strength–Vickers hardness relationship including diamond. Data sources are as follows: W (Brazhkin et al. 2002; He and Duffy 2006), Os (Kenichi 2004; Weinberger et al. 2008) Re (Duffy et al. 1999a; Brazhkin et al. 2002), CaO (Haines et al. 2001; Speziale et al. 2006), CaF_2 (Kavner 2008; Chen et al. 2011), MgO (Khan et al. 1992; Merkel et al. 2002), Olivine (Evans and Goetze 1979; Uchida et al. 1996), Garnet (Sirdeshmukh et al. 2001; Kavner 2007), $MgSiO_3$-Pv (Karato et al. 1990; Shieh et al. 2004), TiN (Kuwahara et al. 2001; Chen et al. 2010a), Ruby (Teter 1998), α-SiC (Qian et al. 2005; Zhang et al. 2002), WB (Chen et al. 2010b; Dong et al. 2012), WB_4 (Mohammadi et al. 2011; Xiong, Unpublished data), TaC (Liermann et al. 2005; Kim et al. 2009), SiO_2-stishovite (Andrievski 2001; Shieh et al. 2002), ReB_2 (Qin et al. 2008; Chung et al. 2007), OsB_2 (Chung et al. 2008; Kavner et al. 2012), TiB_2 (Munro 2000; Amulele et al. 2006), γ-Si_3N_4 (Jiang et al. 2001; Kiefer et al. 2005), B_6O (He et al. 2002, 2004), c-BC_2N (Zhao et al. 2002; Dong et al. 2009), and diamond (Vepřek et al. 2000; Eremets et al. 2005)

previous radial X-ray diffraction measurements of Al_2O_3 with Al_2O_3–Al composites oriented horizontally along the radial direction (Conil and Kavner 2006).

Alumina is important as a hard ceramic material with wide high-temperature and high-pressure applications. In recent years, there has been growing interest in the discovery or synthesis of new hard or superhard solids (Haines et al. 2001; Brazhkin et al. 2002). A superhard material should have a high bulk modulus to resist volume compression, a high shear modulus to resist deformation, and strong resistance to plastic deformation. However, the bulk modulus and shear modulus are known to be insufficient by themselves to predict high hardness (Haines et al. 2001; He et al. 2004; Cumberland et al. 2005). Hardness can vary by more than a factor of ~10 for different materials with similar shear moduli (Haines et al. 2001). Hardness can be measured by indentation of a material by a hard indentor, and the Vickers hardness, H_v, is one of the most frequently used hardness scales. The measurement process for Vickers hardness is qualitatively similar to the uniaxial loading of a sample in the DAC. The sample deforms plastically, i.e., yields, under loading by diamonds in both cases. In Fig. 6, we summarize measurements of the Vickers hardness at ambient pressure and the high-pressure yield strength of ceramic materials and strong metals from selected static DAC experiments using radial X-ray diffraction. Among ceramic materials, a positive correlation can be observed between the high-pressure yield strength and Vickers hardness that is approximately linear with pressures [although a nonlinear relation is required if diamond is also included (see inset)]. The strong metals (W, Os, Re) follow a shallower trend. The very low yield strength of stishovite may be due to weakening associated with its phase transition (Shieh et al. 2002). In addition, the behavior of diamond may be an exception as indentation hardness measurements require the indenter to be harder than the measured sample. As diamond is the hardest known material, the measurement of hardness (as well as yield strength) is more complicated and difficult. The general relationship shown in Fig. 6 is useful for predicting the strength of materials at

high pressures, as well as for evaluating potential superhard solids based on static high-pressure strength measurements.

Conclusions

The lattice strain and stress state of polycrystalline ruby were investigated up to 68.1 GPa under non-hydrostatic compression by angle-dispersive X-ray diffraction in a radial geometry in a diamond anvil cell. Knowledge of the stress state of ruby under high pressure will be helpful for evaluating how non-hydrostatic stress could bias the pressure measurement from the ruby fluorescence scale under non-hydrostatic conditions. For example, our measurements could be used to help quantify how non-hydrostatic stress affects the ruby fluorescence lines (Chai and Brown 1996). More generally, this work provides a better understanding of the high-pressure mechanical properties of ruby which is an important and widely used material. The ratio of the differential stress to the shear modulus increased with pressure from ~3.4 % at 18.5 GPa to ~6.5 % at 68.1 GPa. These values are similar to those observed in other oxides and silicates of geophysical relevance. A maximum differential stress of ~16 GPa can be supported by ruby at 68.1 GPa. The increase in differential stress with pressure obtained in this work is similar to results from high-strain-rate shock compression but is greater than that determined from the pressure gradient method in the diamond anvil cell. Through a synthesis of high-pressure yield strength measurements on a range of strong solids, we show a correlation between static yield strength and Vickers hardness that provides an useful guideline to relate the hardness at ambient conditions with high-pressure yielding behavior. Thus, the high-pressure yield strength can be used as a proxy for material hardness.

Acknowledgments We thank Z. Chen and X. Hong of Stony Brook University for experimental assistance. This work was supported by the National Natural Science Foundation of China (Grants Nos. 11027405 and 10976018), China 973 Program (Grant No. 2011CB808200),the Carnegie-DOE Alliance Center, and the U.S. National Science Foundation. Use of X17C, National Synchrotron Light Sources was supported by COMPRES, the Consortium for Materials Properties Research in Earth Sciences under NSF Cooperative Agreement No. EAR 11-57758, and by the U.S. Department of Energy, Office of Science, Office of Basic Energy Sciences under Contract No. DE-AC02-98CH10886.

References

Amulele GM, Manghnani MH, Somayazulu M (2006) Application of radial x-ray diffraction to determine the hydrostatic equation of state and strength of TiB_2 up to 60 GPa. J Appl Phys 99:023522

Andrievski RA (2001) Superhard materials based on nanostructured high-melting point compounds: achievements and perspectives. Int J Refract Met Hard Mater 19:447–452

Brazhkin VV, Lyapin AG, Hemley RJ (2002) Harder than diamond: dreams and reality. Philos Mag 82:231–253

Chai M, Brown JM (1996) Effects of static non-hydrostatic stress on the R lines of ruby single crystals. Geophys Res Lett 23:3539–3542

Chen H, Peng F, Mao HK, Shen G, Liermann HP, Li Z, Shu J (2010a) Strength and elastic moduli of TiN from radial x-ray diffraction under nonhydrostatic compression up to 45 GPa. J Appl Phys 107:113503

Chen Y, He D, Qin J, Kou Z, Wang S, Wang J (2010b) Ultrahigh-pressure densification of nanocrystalline WB ceramics. J Mater Res 25:637

Chen MJ, Jiang WB, Cheng J, Chu X (2011) Research on the mechanical properties of CaF_2 crystal for ultra-precision machining. Solid State Phenom 175:77–81

Chervin JC, Canny B, Mancinelli M (2001) Ruby-spheres as pressure gauge for optically transparent high pressure cells. High Press Res 21:305–314

Chijioke AD, Nellis WJ, Soldatov A, Silvera IF (2005) The ruby pressure standard to 150 GPa. J Appl Phys 98:114905

Chung DH, Simmons G (1968) Pressure and temperature dependences of the isotropic elastic moduli of polycrystalline alumina. J Appl Phys 39:5316

Chung H-Y, Weinberger MB, Levine JB, Kavner A, Yang JM, Tolbert SH, Kaner RB (2007) Synthesis of ultra-incompressible superhard rhenium diboride at ambient pressure. Science 316:436–439

Chung H-Y, Yang JM, Tolbert SH, Kaner RB (2008) Anisotropic mechanical properties of ultra-incompressible, hard osmium diboride. J Mater Res 23:1797–1801

Conil N, Kavner A (2006) Elastic behavior and strength of Al_2O_3 fiber/Al matrix composite and implications for equation of state measurements in the diamond anvil cell. J Appl Phys 100:043517

Cumberland RW, Weinberger MB, Gilman JJ, Clark SM, Tolbert SH, Kaner RB (2005) Osmium diboride, an ultra-incompressible, hard material. J Am Chem Soc 127:7264

Dewaele A, Loubeyre P, Mezouar M (2004) Equations of state of six metals above 94 GPa. Phys Rev B 70:094112

Dong H, He D, Duffy TS, Zhao Y (2009) Elastic moduli and strength of nanocrystalline cubic BC_2N from x-ray diffraction under nonhydrostatic compression. Phys Rev B 79:014105

Dong H, Dorfman SM, Chen Y, Wang H, Wang J, Qin J, He D, Duffy TS (2012) Compressibility and strength of nanocrystalline tungsten boride under compression to 60 GPa. J Appl Phys 111:123514

Dorogokupets PI, Oganov AR (2007) Ruby, metals, and MgO as alternative pressure scales: a semiempirical description of shock-wave, ultrasonic, x-ray, and thermochemical data at high temperatures and pressures. Phys Rev B 75:024115

Duffy TS (2007) Strength of materials under static loading in the diamond anvil cell. In: Furnish MD, Elert ML, Russell TP, White CT (eds) Shock compression of condensed matter – 2007. AIP, NY, pp 639–644

Duffy TS, Shen G, Heinz DL, Shu J, Ma Y, Mao HK, Hemley RJ, Singh AK (1999a) Lattice strains in gold and rhenium under nonhydrostatic compression to 37 GPa. Phys Rev B 60:15063

Duffy TS, Shen G, Shu J, Mao HK, Hemley RJ, Singh AK (1999b) Elasticity, shear strength, and equation of state of molybdenum and gold from x-ray diffraction under nonhydrostatic compression to 24 GPa. J Appl Phys 86:6729

Eggert JH, Goettel KA, Silvera IF (1989) Ruby at high pressure. I. Optical line shifts to 156 GPa. Phys Rev B 40:5724–5732

Eremets MI, Trojan IA, Gwaze P, Huth J, Boehler R, Blank VD (2005) The strength of diamond. Appl Phys Lett 87:141902

Evans B, Goetze C (1979) The temperature variation of hardness of olivine and its implication for polycrystalline yield stress. J Geophys Res 1978–2012(84):5505–5524

Fei Y, Ricolleau A, Frank M, Mibe KJ, Shen G, Prakapenka V (2007) Toward an internally consistent pressure scale. Proc Natl Acad Sci 104:9182–9186

Forman RA, Piermarini GJ, Barnett JD, Block S (1972) Pressure measurement made by the utilization of ruby sharp-line luminescence. Science 176:284–285

Funamori N, Yagi T, Uchida T (1994) Deviatoric stress measurement under uniaxial compression by a powder x-ray diffraction method. J Appl Phys 75:4327–4331

Gieske JH, Barsch GR (1968) Pressure dependence of the elastic constants of single crystalline aluminum oxide. Phys Status Solidi B 29:121–131

Haines J, Léger J, Bocquillon G (2001) Synthesis and design of superhard materials. Annu Rev Mater Res 31:1–23

Hammersley A, Svensson S, Hanfland M, Fitch AN, Häusermann D (1996) Two-dimensional detector software: from real detector to idealised image or two-theta scan. High Press Res 14:235

He D, Duffy TS (2006) X-ray diffraction study of the static strength of tungsten to 69 GPa. Phys Rev B 73:134106

He D, Zhao Y, Daemen L, Qian J, Shen TD, Zerda TW (2002) Boron suboxide: as hard as cubic boron nitride. Appl Phys Lett 81:643

He D, Shieh SR, Duffy TS (2004) Strength and equation of state of boron suboxide from radial x-ray diffraction in a diamond cell under nonhydrostatic compression. Phys Rev B 70:184121

Holzapfel WB (2003) Refinement of the ruby luminescence pressure scale. J Appl Phys 93:1813

Jephcoat AP, Hemley RJ, Mao HK (1988) X-ray diffraction of ruby (Al_2O_3:Cr^{+3}) to 175 GPa. Phys B C 150:115–121

Jiang JZ, Kragh F, Frost DJ, Stahl K, Lindelov H (2001) Hardness and thermal stability of cubic silicon nitride. J Phys: Condens Matter 13:L515–L520

Karato S, Fujino K, Ito E (1990) Plasticity of $MgSiO_3$ perovskite: the results of microhardness tests on single crystals. Geophys Res Lett 17:13–16

Kavner A (2007) Garnet yield strength at high pressures and implications for upper mantle and transition zone rheology. J Geophys Res 112:B12207

Kavner A (2008) Radial diffraction strength and elastic behavior of CaF_2 in low- and high-pressure phases. Phys Rev B 77:224102

Kavner A, Duffy TS (2001) Strength and elasticity of ringwoodite at upper mantle pressures. Geophys Res Lett 28:2691

Kavner A, Weinberger MB, Shahar A, Cumberland RW, Levine JB, Kaner RB, Tolbert SH (2012) Lattice strain of osmium diboride under high pressure and nonhydrostatic stress. J Appl Phys 112:013526

Kenichi T (2004) Bulk modulus of osmium: high-pressure powder x-ray diffraction experiments under quasihydrostatic conditions. Phys Rev B 70:012101

Khan MY, Brown LM, Chaudhri MM (1992) The effect of crystal orientation on the indentation cracking and hardness of MgO single crystals. J Phys Appl Phys 25:A257–A265

Kiefer B, Shieh SR, Duffy TS, Sekine T (2005) Strength, elasticity, and equation of state of the nanocrystalline cubic silicon nitride γ-Si_3N_4 to 68 GPa. Phys Rev B 72:014102

Kim B-R, Woo KD, Doh JM, Yoon JK, Shon IJ (2009) Mechanical properties and rapid consolidation of binderless nanostructured tantalum carbide. Ceram Int 35:3395–3400

Klotz S, Chervin J-C, Munsch P, Le Marchand G (2009) Hydrostatic limits of 11 pressure transmitting media. J Phys Appl Phys 42:075413

Kuwahara H, Mazaki N, Takahashi M, Watanabe T, Yang X, Aizawa T (2001) Mechanical properties of bulk sintered titanium nitride ceramics. Mater Sci Eng 319–321:687

Liermann HP, Singh AK, Manoun B, Saxena SK, Zha CS (2005) Compression behavior of $TaC_{0.98}$ under nonhydrostatic and quasi-hydrostatic pressures up to 76 GPa. Int J Refract Met Hard Mater 23:109–114

Mao HK, Bell PM, Shaner JW, Steinberg DJ (1978) Specific volume measurements of Cu, Mo, Pd, and Ag and calibration of the ruby R1 fluorescence pressure gauge from 0.06 to 1 Mbar. J Appl Phys 49:3276

Meade C, Jeanloz R (1988) Yield strength of MgO to 40 GPa. J Geophys Res 93:3261

Meade C, Jeanloz R (1990) Yield strength of Al_2O_3at high pressures. Phys Rev B 42:2532–2535

Merkel S, Wenk HR, Shu J, Shen G, Gillet P, Mao HK, Hemley RJ (2002) Deformation of polycrystalline MgO at pressures of the lower mantle. J Geophys Res 107:2271

Merkel S, Wenk HR, Badro J, Montagnac G, Gillet P, Mao HK, Hemley RJ (2003) Deformation of ($Mg_{0.9}$, $Fe_{0.1}$) SiO_3 perovskite aggregates up to 32 GPa. Earth Planet Sci Lett 209:351–360

Mohammadi R, Lech AT, Xie M, Weaver BE, Yeung MT, Tolbert SH, Kaner RB (2011) Tungsten tetraboride, an inexpensive superhard material. Proc Natl Acad Sci 108:10958–10962

Munro RG (2000) Material properties of titanium diboride. J Res Natl Inst Stand Technol 105:709–720

Nellis WJ, Kanel GI, Razorenov SV, Rajendran AM (2010) Entropy-dominated dissipation in sapphire shock-compressed up to 400 GPa (4 Mbar). J Phys: Conf Ser 215:012148

Piermarini GJ, Block S, Barnett JD, Forman RA (1975) Calibration of the pressure dependence of the R1 ruby fluorescence line to 195 kbar. J Appl Phys 46:2774–2780

Qian J, Daemen LL, Zhao Y (2005) Hardness and fracture toughness of moissanite. Diam Relat Mater 14:1669–1672

Qin J, He D, Wang J, Fang L, Lei l, Li Y, Hu J, Kou Z, Bi Y (2008) Is rhenium diboride a superhard material? Adv Mater 20:4780–4783

Reinhart WD, Chhabildas LC (2003) Strength properties of Coors AD995 alumina in the shocked state. Int J Impact Eng 29:601–619

Reinhart WD, Chhabildas LC, Vogler TJ (2006) Investigating phase transitions and strength in single-crystal sapphire using shock–reshock loading techniques. Int J Impact Eng 33:655–669

Shieh SR, Duffy TS, Li B (2002) Strength and elasticity of SiO_2 across the stishovite–$CaCl_2$-type structural phase boundary. Phys Rev Lett 89:255507

Shieh SR, Duffy TS, Shen G (2004) Elasticity and strength of calcium silicate perovskite at lower mantle pressures. Phys Earth Planet Interiors 143–144:93–105

Singh AK (1993) The lattice strains in a specimen (cubic system) compressed nonhydrostatically in an opposed anvil device. J Appl Phys 73:4278–4286

Singh AK (2004) X-ray diffraction from solids under nonhydrostatic compression—some recent studies. J Phys Chem Solids 65:1589–1596

Singh AK (2009) Analysis of nonhydrostatic high-pressure diffraction data (cubic system): assessment of various assumptions in the theory. J Appl Phys 106:043514

Singh AK, Liermann HP (2011) Strength and elasticity of niobium under high pressure. J Appl Phys 109:113539

Singh AK, Balasingh C, Mao HK, Hemley RJ, Shu J (1998a) Analysis of lattice strains measured under nonhydrostatic pressure. J Appl Phys 83:7567–7575

Singh AK, Mao HK, Shu J, Hemley RJ (1998b) Estimation of single-crystal elastic moduli from polycrystalline X-ray diffraction at high pressure: application to FeO and Iron. Phys Rev Lett 80:2157–2160

Singh AK, Andrault D, Bouvier P (2012) X-ray diffraction from stishovite under nonhydrostatic compression to 70 GPa: strength and elasticity across the tetragonal → orthorhombic transition. Phys Earth Planet Interiors 208–209:1–10

Sirdeshmukh DB, Sirdeshmukh L, Subhadra KG, Rao KK, Laxman SB (2001) Systematic hardness measurements on some rare earth garnet crystal. Bull Mater Sci 24:469–473

Speziale S, Shieh SR, Duffy TS (2006) High-pressure elasticity of calcium oxide: a comparison between Brillouin spectroscopy and radial X-ray diffraction. J Geophys Res 111:B02203

Teter DM (1998) Computational alchemy: the search for new superhard materials. MRS Bull 23:22

Uchida T, Funamori N, Ohtani T, Yagi T (1996) Differential stress of MgO and Mg_2SiO_4 under uniaxial stress field: Variation with pressure, temperature, and phase transition. High Press Sci Technol. Proceedings of the 15th AIRAPT conference, Warsaw, Poland, pp 183–185

Vepřek S, Zeer A, Riedel R (2000) In: Riedel R (ed) Handbook of ceramic hard materials. Wiley-VCH, Weinheim

Vignes RM, Becker R, Stölken J, Kumar M (2013) An assessment of diamond anvil cell measurements on material strength. J Appl Phys 113:213503

Weinberger MB, Tolbert SH, Kavner A (2008) Osmium metal studied under high pressure and nonhydrostatic stress. Phys Rev Lett 100:45506

Zhang JZ, Wang LP, Weidner DJ, Uchida T, Xu JA (2002) The strength of moissanite. Am Miner 87:1005

Zhao Y, He DW, Daemen LL, Shen TD, Schwarz RB, Zhu Y, Bish DL, Huang J, Zhang J, Shen G, Qian J, Zerda TW (2002) Superhard B–C–N materials synthesized in nanostructured bulks. J Mater Res 17:3139–3145